

# Design and In-Situ Characterization of Catalyst Surfaces

Department of Materials Molecular Science  
Division of Electronic Structure



TADA, Mizuki	Associate Professor
MURATSUGU, Satoshi	Assistant Professor
MAITY, Niladri	Post-Doctoral Fellow
ZHANG, Shenghong	Post-Doctoral Fellow
SAIDA, Takahiro	Post-Doctoral Fellow
WAKI, Minoru	Post-Doctoral Fellow
SODE, Aya	Post-Doctoral Fellow
THUMRONGPATANARAKS, Wipavee	JENESYS Program Visiting Scientist
GAN, Raymond	Visiting Scientist*
JIANG, Lu	Visiting Scientist*
LIM, Min Hwee	Visiting Scientist*
WANG, Fei	Graduate Student
ISHIGURO, Nozomu	Graduate Student†
FUNAKI, Yukino	Technical Fellow
USUI, Chika	Technical Fellow
GONDO, Makiko	Technical Fellow
FUKUTOMI, Yukiyo	Secretary

## 1. Preparation and Catalytic Performances of a Molecularly Imprinted Ru-Complex Catalyst with an NH<sub>2</sub> Binding Site on SiO<sub>2</sub>

The potential of immobilized metal-complex catalysts remarkably interplays with the nature of support surfaces, resulting in significant rate enhancements and unique catalytic performances that their homogeneous counterparts do not exhibit. We proposed the design of molecularly imprinted metal-complex catalysts on SiO<sub>2</sub> surfaces, whose ligand was used as a template, and molecularly imprinted metal-complex catalysts have been applied for selective catalysis.

Natural enzymes, which are quite selective catalysts for particular reactants, possess highly sophisticated catalytic systems with active metal species, shape-selective reaction space, and molecular recognition sites spatially arranged for the particular reactants. Artificial design of such a sophisticated catalytic system is still difficult and the preparation of both catalytically active site and shape-selective reaction space with spatially arranged molecular binding sites. We have prepared a molecularly imprinted Ru-complex catalyst with NH<sub>2</sub> binding site on the wall of a molecularly imprinted cavity toward the shape-selective transfer hydrogenation catalysis.<sup>1)</sup>

A template alcohol, which was the template for *o*-fluorobenzophenone hydrogenation, was coordinated to a SiO<sub>2</sub>-supported Ru complex (Ru-*N-p*-styrenesulfonyl-1,2-diphenylethylenediamine) and the hydrolysis polymerization of tetramethoxysilane produced SiO<sub>2</sub>-matrix overlayers surrounding the supported Ru complex on the surface. A carbamate group (-NHCOO-) connected to a silane-coupling moiety (-Si(OC<sub>2</sub>H<sub>5</sub>)<sub>3</sub>) was tethered to the alcohol template and the cleavage of the carbamate moiety after hanging the silane-

coupling branch on the wall of a molecularly imprinted cavity produced a spatially arranged NH<sub>2</sub> binding site for the hydrogenation of *o*-fluorobenzophenone as shown in Figure 1.

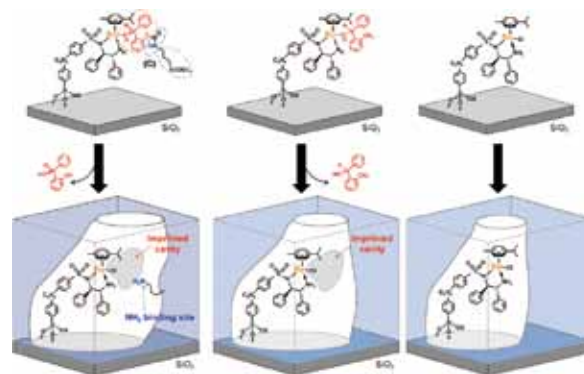


**Figure 1.** Preparation of molecularly imprinted Ru catalysts with an imprinted cavity with an NH<sub>2</sub> binding site on the wall of the cavity, with an imprinted cavity without an NH<sub>2</sub> binding site, and without an imprinted cavity.

We prepared three catalysts with a molecularly imprinted cavity with an NH<sub>2</sub> binding site, with a molecularly imprinted cavity without an NH<sub>2</sub> binding site, and without a cavity of the template illustrated in Figure 1. The catalytic performances of the transfer hydrogenation of *o*-fluorobenzophenone were significantly different between these three catalysts under identical reaction conditions. The transfer hydrogenation did not proceed at all on the catalyst prepared without the template. On the other hand, other two catalysts prepared with the templates exhibited activity for the hydrogenation, but we

found differences in the hydrogenation rates of *o*-fluorobenzophenone and *o*-methylbenzophenone. These two reactants have similar shapes to each other, but *o*-fluorobenzophenone with F group, which can interact to the NH<sub>2</sub> binding site by hydrogen bonding, was preferably hydrogenated on the molecularly imprinted catalyst with the NH<sub>2</sub> binding site. Such differences in the hydrogenation activity were not observed on the imprinted catalyst without the NH<sub>2</sub> binding site. The NH<sub>2</sub> binding site promoted the preferable adsorption of the specific molecule that can interact with the molecular binding site, resulting in increase in the transfer hydrogenation activity. The strategy is promising to create an artificial enzymatic catalyst surfaces in the future.

## 2. Operando Time-Resolved XAFS for Surface Events on Pt<sub>3</sub>Co/C and Pt/C Cathode Catalysts in Practical PEFCs during Voltage-Operating Processes

Polymer electrolyte fuel cells (PEFCs) are among the most efficient clean energy technologies, but practical application in automobiles remains challenging because of the high cost and insufficient durability of cathode catalysts. To improve fuel-cell performance and cathode catalyst durability, alloying of Pt with 3d transition metal elements is a promising approach. Pt-Co alloy is a representative of the Pt-alloy cathode catalysts and has been reported to be more active and durable than Pt/C catalysts. Although electrochemical surface events have been extensively investigated, the structural kinetics of the transformations of catalyst themselves and the ORR reaction mechanism on practical Pt-Co catalysts have not been established. *In situ* time-resolved QXAFS spectra at the Pt L<sub>III</sub>-edge and Co K-edge were measured at 500 ms intervals, and the analysis of the series of the operando QXAFS spectra for the PEFC bimetal cathode catalyst revealed the rate constants of electron transfer, changes in the charge density of Pt<sub>3</sub>Co nanoparticles, and changes in the local coordination structures with Pt–Pt, Pt–Co, Co–Co, and Pt–O bonds for the first time (Table 1).<sup>2)</sup>

We compared the reaction mechanism and structural kinetics on the Pt<sub>3</sub>Co/C and Pt/C catalysts under similar fuel-cell operating conditions. It is to be noted that all the rate constants on the Pt<sub>3</sub>Co/C catalyst were larger than the corresponding rate constants on the Pt/C catalysts. During the 1.0 V → 0.4 V process, for example, Pt–Pt bond breaking on the Pt<sub>3</sub>Co/C catalyst was 1.5-fold to that on the Pt/C catalyst. The rate constant of Pt–O bond breaking ( $k'_{\text{Pt-O}}$ ), which is highly related to the ORR activity of the cathode catalyst, was about 4 times higher on Pt-Co/C (0.4 s<sup>-1</sup>) than on Pt/C (0.11 s<sup>-1</sup>).

### Award

ISHIGURO, Nozomu; Student Presentation Award (JXAFS 14).

There were also a significant difference in the rate constant of Pt–Pt bond re-formation ( $k'_{\text{Pt-Pt}}$ ), on Pt<sub>3</sub>Co/C (0.3 s<sup>-1</sup>) and Pt/C (0.078 s<sup>-1</sup>), which may be relevant for realizing better catalyst durability of the Pt<sub>3</sub>Co/C catalyst.

The irreversible oxidation of the Pt catalysts depends on the difference in rate between oxidation and reduction of the Pt catalysts during voltage cycling. The repeated cycling on oxidized Pt species which could not be recovered causes extensive dissolution of the Pt cathode catalyst. Pt<sub>3</sub>Co alloy systems facilitate reversible oxidation/reduction in the voltage-cycling processes. The structural kinetics determined from the *in situ* time-resolved XAFS revealed that all the rate constants of the surface events on the Pt<sub>3</sub>Co/C cathode catalyst were higher than those on Pt/C, particularly the reduction steps involving Pt–O bond breaking. Reversible redox cycles on Pt<sub>3</sub>Co alloys are suggested as a key factor in the superior performance of Pt<sub>3</sub>Co alloy cathode catalysts in PEFCs. Understanding of the fundamental issues of the structural kinetics of the catalyst surface events by *in situ* time-resolved XAFS establishes new boundaries for the regulation and operation of fuel cells.

**Table 1.** Rate constants for Pt<sub>3</sub>Co/C and Pt/C MEAs in voltage-cycling processes by operando time-resolved XAFS.

Process		Rate constant /s <sup>-1</sup>	
		Pt <sub>3</sub> Co/C	Pt/C
0.4 → 1.0 V	XANES		
	white-line height	0.12 ± 0.02	0.073 ± 0.001
	CN (Pt–Pt)	0.13 ± 0.03	0.088 ± 0.008
	CN (Pt–Co)	No change	–
	CN (Pt–O)	0.10 ± 0.03	0.076 ± 0.009
charge in the fuel cell		2.86 ± 0.04	1.84 ± 0.02
		0.258 ± 0.003	0.167 ± 0.001
1.0 → 0.4 V	XANES		
	white-line height	0.24 ± 0.05	0.14 ± 0.03
	CN (Pt–Pt)	0.3 ± 0.1	0.078 ± 0.009
	CN (Pt–Co)	No change	–
	CN (Pt–O)	0.4 ± 0.2	0.11 ± 0.02
charge in the fuel cell		3.68 ± 0.03	2.16 ± 0.01
		0.484 ± 0.002	0.259 ± 0.001

### References

- 1) Y. Yang, Z. Weng, S. Muratsugu, N. Ishiguro, S. Ohkoshi and M. Tada, *Chem. –Eur. J.* **18**, 1142–1153 (2012).
- 2) N. Ishiguro, T. Saida, T. Uruga, O. Sekizawa, S. Nagamatsu, K. Nitta, T. Yamamoto, S. Ohkoshi, Y. Iwasawa, T. Yokoyama and M. Tada, *ACS Catal.* **2**, 1319–1330 (2012).

\* IMS International Collaboration Program

† carrying out graduate research on Cooperative Education Program of IMS with The University of Tokyo